

Distinguishing Phases via Non-Markovian Dynamics of Entanglement in Topological Quantum Codes under Parallel Magnetic Field

Harikrishnan K. J. and Amit Kumar Pal

Department of Physics, Indian Institute of Technology Palakkad, Palakkad 678 557, India

(Dated: August 26, 2021)

We investigate the dynamics of localizable entanglement and its lower bounds on non-trivial loops of topological quantum codes with parallel magnetic field under single-qubit dephasing noise. We identify a specific measurement basis that optimizes the lower bound of localizable entanglement when measurement is restricted to single-qubit Pauli measurements only, and provides a non-trivial lower bound in the presence of dephasing noise. We also define a resource-optimized lower bound that can be computed for larger systems according to the computational resource in hand. These lower bounds are shown to exhibit specific dynamical features at large time under Markovian and non-Markovian single-qubit dephasing noise, which can be utilized to distinguish the topological phase of the system from the non-topological phase. More specifically, we demonstrate that under non-Markovian dephasing noise, at a large time, the non-topological phase can be identified by large amplitude oscillations of the lower bound as a function of the strength of the parallel magnetic field. We also show that the dynamics can be used to identify the Markovian and Non-Markovian nature of the single-qubit dephasing noise if the phase information about system is available.

I. INTRODUCTION

The world-wide drive for achieving quantum supremacy [1–3] and for implementing large-scale fault-tolerant quantum computers [4] in the last couple of decades have established topological quantum error correcting codes [5, 6], eg. the Kitaev code [7, 8] and the color code [9] as ideal candidate systems for the task. Robustness of these systems against loss of physical qubits [10], and computational errors [6, 11, 12] has motivated realizations of these systems in the laboratory using substrates like trapped ions [13, 14] and superconducting qubits [15], which has made experimental verification of theoretical results possible. Moreover, with the introduction of noisy intermediate-scale quantum devices built using 50-100 physical qubits [16], and their use towards the goal of achieving quantum supremacy [3], the importance of topological quantum codes hosting a large number of qubits has now been established in the context of building large quantum memories [7] and successfully implementing quantum error correction protocols for errors on multiple physical qubits [5, 6].

The possibility of adverse effects of local perturbations in quantum computation tasks has motivated investigations of topological quantum codes as lattice models [11, 17–21], where perturbations in the form of external magnetic fields [11, 17, 18, 21] and spin-spin interactions [19, 21] are considered. The ground state of the system retains the topological order [22, 23] when the external perturbation is small, while with increasing perturbation strength, a topological to non-topological quantum phase transition takes place, the quantum phase transition point being a quantifier of the robustness of the code corresponding to the perturbation parameter. In contrast to the Landau paradigm of descriptions of phases and order parameters [24], topological to non-topological phase transitions can not be characterized by local order parameters and spontaneous symmetry breaking [23]. While studies of the topological to non-topological quantum phase transitions in locally perturbed topological quantum codes has so far been carried out in terms of ground state

energy per site and the single-particle gap [11, 17–21], the importance of the sustenance of the topological order against local perturbations in the quantum information processing and quantum computation [5, 6] highlights the necessity of investigations of these systems in terms of quantum correlation measures that are resources in quantum protocols [25, 26].

Along with serving as resource in quantum protocols like teleportation [25, 27], dense-coding [25, 28], quantum cryptography [25, 29], and measurement-based quantum computation [25, 29], entanglement [25] is by far the most widely accepted quantum correlation for characterizing quantum many-body systems [30], including non-topological [30–32] and topological phases [8, 33] of lattice models. Advancement in the investigation of biparty- and multiparty-entangled quantum states in the laboratory using trapped ions [34] and superconducting qubits [35] has brought testing of theoretical results on entanglement in characterizing phases of perturbed topological quantum codes within our grasp. In this line of investigation, a number of challenges have been prominent. The fact that topological phases are characterized by non-local order parameters [22, 23] indicates the requirement of investigating multipartite entanglement [25] in the ground state(s) of the system, or in the reduced state of a chosen subsystem, which is difficult due to the scarcity of computable multipartite entanglement measures [25]. Also, partial trace-based approach of computing entanglement over a chosen subsystem of topological quantum codes by determining its reduced state from the ground state of the entire system fails as tracing out the degrees of freedom of the spins in the rest of the system results in diagonal density matrices, thereby leading to vanishing entanglement [25, 36]. Moreover, inevitable interaction of the system with environment [37] leads to a rapid decay of entanglement over time [38], making it difficult to investigate the phase structure of the perturbed topological quantum code in terms of entanglement at a latter time in the realistic scenario. Although the effect of thermal noise on entanglement in unperturbed topological quantum codes has been investigated [39], trends of entanglement in these systems in the presence of noise as well as local perturbations in the form of

magnetic field or spin-spin interaction remain unexplored.

In this paper, we address the question as to whether the topological and non-topological phases and the corresponding quantum phase transition can be investigated in terms of appropriate entanglement measures in the presence of decoherence in the system. More specifically, we assume a situation where each of the qubits in the system is subjected to local Markovian and non-Markovian dephasing noise [40–42], and ask if the topological and non-topological phases can be distinguished during the evolution of the system. We consider topological quantum codes, such as the Kitaev code and the color code, in the presence of a parallel magnetic field [17, 21], and quantify entanglement over a multipart subsystem of the code via a local measurement-based protocol [43–46], where a *localizable entanglement* [44] can be computed over a chosen subsystem by maximizing the average entanglement over the subsystem with respect to all possible single-qubit projection measurements performed on all the qubits in the rest of the system. The choice of such a measure of entanglement is based on the recent results on the multipart nature of localizable entanglement [47], and the requirement for a non-local order parameter to characterize the topological phase of the system. We show that apart from being useful in introducing concepts like correlation length in low-dimensional quantum spin models [45], characterizing phases in cluster-Ising [31] and cluster-XY models [32], and as the key resource in protocols like measurement-based quantum computation [29] and entanglement percolation [48], the dynamics of localizable entanglement under single-qubit Markovian and non-Markovian dephasing noise can also distinguish between the topological and non-topological phases in topological quantum codes in parallel magnetic field.

To tackle the difficulty of computing the localizable entanglement over a chosen subsystem due to the measurement-based optimization involved in its definition [44, 45], we numerically compute a number of lower bounds in topological quantum codes of increasing sizes (cf. [36]), as a function of the strength of the parallel magnetic field and time, over non-trivial loops on the lattice under periodic boundary condition. We identify a canonical setup of Pauli measurements which optimizes the lower bound of localizable entanglement when measurements are restricted to single-qubit Pauli measurements, and performs well in providing a lower bound even in the presence of the dephasing noise. Using the canonical measurement setup, we define a resource-optimized lower bound which can be computed for larger systems, and test its performance in the case of Kitaev code of large size with parallel magnetic field.

We show that in the presence of non-Markovian single-qubit dephasing noise on all qubits due to their connection with local baths constituted of simple harmonic oscillators with Ohmic spectral function [41, 42], at a large time, the lower bounds of localizable entanglement exhibits rapid oscillation with high amplitude as a function of the strength of the parallel magnetic field in the non-topological phase. This is in contrast to the absence of such oscillating behavior of the lower bounds of localizable entanglement in the topological phase, thereby distinguishing the two phases. The oscillation

increases with an increase in the value of the Ohmicity parameter corresponding to the dephasing noise. We also define an entanglement collapse time depending on the time taken by the localizable entanglement and its lower bounds to reach the first minimum on the t axis during their dynamics, and demonstrate that the entanglement collapse time as a function of the field strength in the case of the Markovian dephasing noise exhibits an increase in the non-topological phase.

The paper is organized as follows. In Sec. II A, we provide brief introductions of the topological quantum codes, including the Kitaev code and the color code, in the presence of parallel magnetic field. Sec. II B describes single-qubit dephasing noise and the corresponding quantum master equation. The definitions of localizable entanglement and its lower bounds are included in Sec. II C. In Sec. III, we discuss the optimal basis for computing localizable entanglement in the noiseless scenario, and introduce the canonical measurement setup. We also define the resource-optimized lower bound of localizable entanglement and discuss its performance for large topological codes. Sec. IV describes the behaviour of localizable entanglement and its lower bounds as a function of time, and discusses how the dynamics can be used to distinguish between the topological and the non-topological phases of the model after a large time has elapsed. Sec. V has concluding remarks.

II. MODELS AND METHODOLOGY

In this Section, we provide a brief overview of the topological codes in the presence of parallel magnetic field. We also discuss the Markovian and non-Markovian dephasing noise, and define localizable entanglement as the appropriate measure for entanglement in topological quantum codes.

A. Topological codes in parallel magnetic field

Kitaev code in a parallel magnetic field. Let us consider a 2D rectangular lattice where the sets of all edges and plaquettes are denoted by \mathcal{N}_E and \mathcal{N}_P respectively, hosting a total of N qubits represented by spin- $\frac{1}{2}$ particles. The lattice is constructed on a $N_P^h \times N_P^v$ architecture, where N_P^h (N_P^v) is the number of plaquettes in the horizontal (vertical) direction, such that $N_P = N_P^h N_P^v$ is the total number of plaquettes in the system (see Fig. 1(a)). Each qubit in the system is situated on an edge of the lattice. Two types of stabilizer operators – the plaquette operators S_p and the vertex operators S_v – are defined on this lattice as

$$S_p = \bigotimes_{i \in p} \sigma_i^z, S_v = \bigotimes_{i \in v} \sigma_i^x, \quad (1)$$

where σ_i^x (σ_i^z) is the x (z) component of Pauli matrices, and p (v) is the plaquette (vertex) index. The plaquette (vertex) operator S_p (S_v) has support on the qubits forming the plaquette p (connected directly to the vertex v) of the square lattice. The Hamiltonian describing the Kitaev model under a parallel

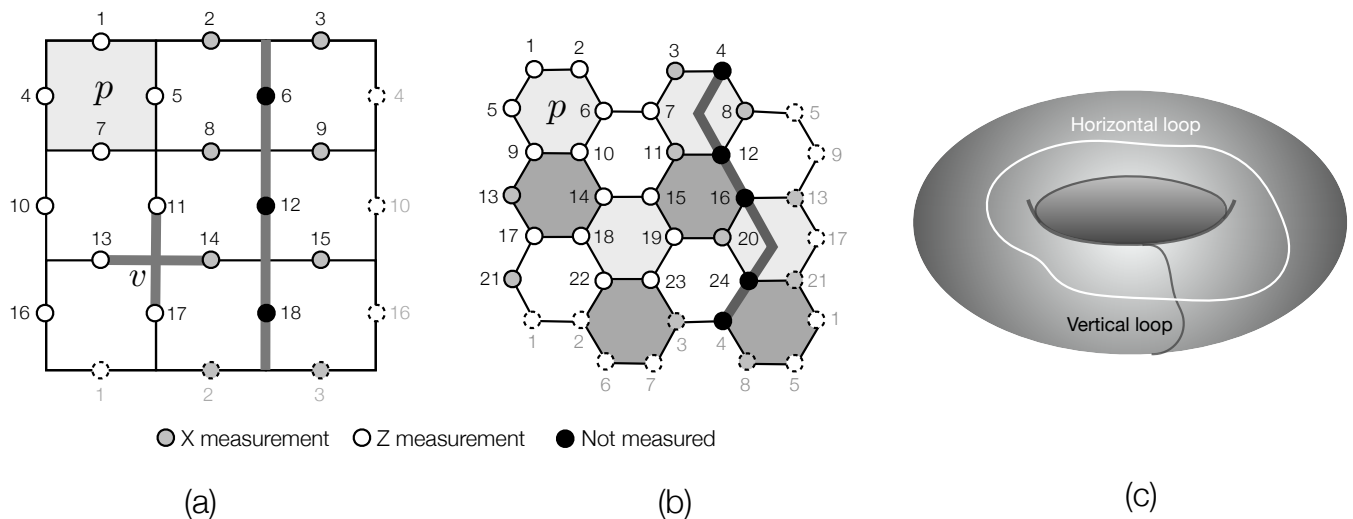


FIG. 1. (Color online) **(a) A Kitaev code on a square lattice of 3×3 architecture.** Each of the N_E edges in the square lattice of N_P plaquettes contains a qubit, represented by the circles, constituting an N -qubit ($N = N_E = 2N_P = 18$ in the present case, with $N_P^h = N_P^v = 3$) system with periodic boundary conditions in both horizontal and vertical directions. Here, N_E (N_P) is the cardinality of \mathcal{N}_E (\mathcal{N}_P) (see Sec. II). A plaquette is denoted by the index p (shown by a shaded plaquette), and a vertex is denoted by the index v (shown by thick gray intersecting lines). A non-trivial loop in the vertical direction has been marked with the thick gray line, consisting of three qubits (represented by black circles). Qubits denoted by dashed circles as outlines are in accordance with the periodic boundary condition. The canonical measurement setup (see Sec. III) here is represented by the σ^x measurements on qubits corresponding to lattice links converging on the non-trivial loop (represented by the gray circles), and σ^z measurement on the rest of the qubits (represented by white circles). The qubits represented by the black circles remain unmeasured. **(b) Color code on a hexagonal lattice.** The lattice is constituted of N_P plaquettes (in the present case, $N_P = 12$ in a 4×3 architecture) and N (in this example, $N = 24$) qubits. Three shades of gray signify three different colors of the plaquettes. The thick gray line represents a vertical non-trivial loop constituted of 4 qubits, marked in black color. The periodic boundary condition in both vertical and horizontal directions are incorporated by marking the repeated qubits with dashed boundaries. The canonical measurement setup (see Sec. III) in this case is given by σ^x measurements on qubits having a direct lattice link with the non-trivial loop (denoted by gray circles), and σ^z measurements on the rest of the qubits (represented by white circles). **(c) A torus of genus 1.** The horizontal and the vertical non-trivial loops are shown by the white (horizontal) and gray (vertical) lines.

magnetic field is given by [17]

$$H_K = -J_P \sum_p S_p - J_V \sum_v S_v - h \sum_{i=1}^N \sigma_i^z, \quad (2)$$

where J_P and J_V are respectively the plaquette and the vertex interaction strengths, and h is the strength of the external magnetic field on every spin. We focus on the parameter subspace defined by $J_P = J_V = J > 0$. In the limit $h/J \rightarrow 0$, the Hamiltonian in Eq. (2) represents the Kitaev model [7, 8].

Under periodic boundary condition, Kitaev model on a square lattice can be embedded on the surface of a torus of genus 1 (see Fig. 1(c)), which holds two non-trivial loops in horizontal and vertical directions. Let us denote the sets of qubits supporting these non-trivial loops in the horizontal and vertical directions by \mathcal{S}_h and \mathcal{S}_v , respectively. Four non-trivial loop operators corresponding to these loops can be defined as

$$L_\alpha^x = \bigotimes_{i \in \mathcal{S}_\alpha} \sigma_i^x, L_\alpha^z = \bigotimes_{i \in \mathcal{S}_\alpha} \sigma_i^z, \quad (3)$$

where $\alpha = h, v$, denoting horizontal and vertical loops, respectively. The Kitaev model has a four-fold degenerate ground state, each of which is an entangled state, which can

be constructed by applying the non-trivial loop operators on

$$|\psi\rangle = \frac{1}{2^N} \prod_v [I + S_v] |0\rangle^{\otimes N}, \quad (4)$$

as

$$|\psi\rangle_g = (L_h^x)^a (L_v^x)^b |\psi\rangle, \quad (5)$$

with $a, b = 0, 1$, where $\{|0\rangle, |1\rangle\}$ is the computational basis in the qubit Hilbert space [21]. With the application of the parallel magnetic field, the ground state degeneracy is lifted, and a non-degenerate ground state of H_K is obtained. The limit $h/J \rightarrow \infty$ corresponds to a fully separable ground state of the form $|1\rangle^{\otimes N}$. With increasing the strength of the parallel magnetic field h , there is a topological to non-topological quantum phase transition at the critical value $g_c = 0.328474(3)$ [17] of the dimensionless system parameter $g = \frac{h}{J}$, which can be determined by identifying the equivalence of the model with the 2D transverse-field Ising model.

Color code in a parallel field. Color codes are topological quantum error correcting codes defined on three-colorable trivalent lattices. The qubits, represented by spin- $\frac{1}{2}$ particles, are situated on the vertices of the lattice [9]. On each plaque-

tte, two types of stabilizer operators are defined as

$$S_p^z = \bigotimes_{i \in p} \sigma_i^z, S_p^x = \bigotimes_{i \in p} \sigma_i^x, \quad (6)$$

where p is the plaquette index. The color code Hamiltonian in the presence of a parallel magnetic field on a hexagonal lattice is given by [21]

$$H_C = -J \sum_p (S_p^x + S_p^z) - h \sum_{i=1}^N \sigma_i^x, \quad (7)$$

where J is the plaquette interaction strength. We consider a hexagonal lattice (see Fig. 1(b)) where the plaquettes can be coded with three different colors such that no two adjacent plaquette has the same color. Similarly, the lattice links can also be colored with the same three colors such that link of a specific color connects plaquettes of the same color. In this paper, we assume $J > 0$. The color code Hamiltonian is obtained from H_C in the $h/J \rightarrow 0$ limit.

Similar to the square lattice, the hexagonal lattice can also be embedded on the surface of a torus of genus 1 under periodic boundary condition, and sets of qubits, denoted by \mathcal{S}_h^c and \mathcal{S}_v^c and constituting two non-trivial loops made of links of each of the three colors, can be identified, where $c \in \{c_1, c_2, c_3\}$ denotes the color index. Using these qubits, six fundamental non-trivial loop operators can be constructed as

$$L_{\alpha,c}^x = \bigotimes_{i \in \mathcal{S}_\alpha^c} \sigma_i^x, L_{\alpha,c}^z = \bigotimes_{i \in \mathcal{S}_\alpha^c} \sigma_i^z. \quad (8)$$

Successive applications of these non-trivial loop operators on

$$|\psi\rangle = \frac{1}{2^N} \prod_p [I + \mathcal{S}_p^x] |0\rangle^{\otimes N}, \quad (9)$$

as

$$|\psi\rangle_g = (L_{h,c_1}^x)^{a_1} (L_{h,c_2}^x)^{a_2} (L_{v,c_1}^x)^{b_1} (L_{v,c_2}^x)^{b_2} |\psi\rangle, \quad (10)$$

$a_1, a_2, b_1, b_2 = 0, 1$ and c_1, c_2 being any two of the three colors, generates the ground state manifold $|\psi\rangle_g$ of the $h/J \rightarrow 0$ limit of the Hamiltonian, consisting of 16 degenerate entangled states [21]. On the other hand, a fully polarized ground state is found at $h/J \rightarrow \infty$, with all spins pointing in the field direction. The topological to non-topological quantum phase transition occurring with increasing h/J can be determined by mapping the model to a Baxter Wu model in a transverse field on a triangular lattice, where The critical value of the dimensionless system parameter $g = \frac{h}{J}$ is $g_c = 0.385$ [21].

B. Dynamics under dephasing noise

Let us now consider a situation where each of the spin- $\frac{1}{2}$ particles in the system starts interacting with a bath from a collection of identical and independent thermal baths at time $t = 0$. Each bath is made of harmonic oscillators, with a bath Hamiltonian given by $H_b = \sum_k \omega_k a_k^\dagger a_k$, where ω_k

is the frequency of the k th bath-mode, and a_k^\dagger (a_k) is the creation (annihilation) operator corresponding to the mode k . The interaction between each spin and its bath is given by $H_{sb} = \sum_k \sigma^z \otimes (g_k a_k + g_k^* a_k^\dagger)$, where g_k is the coupling constant between the spin variable and the k th mode of the bath, such that in the continuum limit, $\sum_k |g_k|^2$ goes to $\int f(\omega) \delta(\omega_k - \omega) d\omega$, $f(\omega)$ being the spectral function of the bath. Assuming that each spin interacts with its own bath only and is immune to the effects of the remaining baths, and considering thermal initial state of the bath, the time-local quantum master equation that governs the dynamics of the system is given by [40–42]

$$\dot{\rho} = -\frac{i}{\hbar} [H, \rho] + \gamma(t) \sum_{i=1}^N (\sigma_i^z \rho \sigma_i^z - \rho). \quad (11)$$

Here, H is the system Hamiltonian H_K (Eq. (2)) or H_C (Eq. (7)), depending on the choice of the system, and ρ is the N -qubit state of the system. The time-dependent dephasing rate $\gamma(t)$ is the same for all qubits, and is given by [42]

$$\gamma(t) = \omega_c [1 + (\omega_c t)^2]^{-\frac{s}{2}} \sin[s \tan^{-1}(\omega_c t)] \Gamma(s), \quad (12)$$

where $\Gamma(s) = \int_0^\infty x^{s-1} e^{-x} dx$ is the Euler Gamma function, ω_c is the cut-off frequency of the bath, and s is the Ohmicity parameter whose value determines whether the bath is sub-Ohmic ($s < 1$), Ohmic ($s = 1$), or super-Ohmic ($s > 1$). At the zero temperature limit of the bath, the value of $s \leq 2$ ensures Markovian spin-bath interaction, while non-Markovianity emerges for $s > 2$ [41, 42]. The critical value $s_c = 2$ for the Markovian to non-Markovian transition on the Ohmicity parameter increases with increasing temperature of the bath. In this paper, we focus on the zero temperature limit of the bath, and unless otherwise stated, we fix the bath cut-off frequency to be $\omega_c = 1$.

Solving Eq. (11), the state of the system $\rho(t)$, as a function of t , can be obtained, and the relevant quantities can subsequently be calculated. In the rest of the paper, we will employ the dimensionless system parameter $g = \frac{h}{J}$, dimensionless time $t \rightarrow \frac{Jt}{\hbar}$ and dimensionless temperature $T \rightarrow \frac{k_B T}{J}$ for describing the system and its dynamics.

C. Localizable entanglement

Localizable entanglement (LE) [44, 45] over a selected subset of qubits in the system is defined as the maximum average entanglement localized over the selected set of qubits via local projection measurements on all the other qubits, and is expressed as

$$E_\Omega^L = \max_{\{M_{\bar{\Omega}}\}} \sum_k p_k E(\rho_\Omega^k). \quad (13)$$

Here, $\{M_{\bar{\Omega}}\}$ is the complete set of single-qubit projection measurements performed over all the qubits in the set $\bar{\Omega}$, Ω is the set of selected qubits over which the localizable entanglement is to be computed such that $\Omega \cup \bar{\Omega}$ represents the entire

system, $\Omega \cap \bar{\Omega} = \emptyset$, and $\rho_{\Omega}^k = \text{Tr}_{\bar{\Omega}}[\rho^k]$, with

$$p_k = \frac{1}{p_k} [(M_{\bar{\Omega}} \otimes I_{\Omega}) \rho (M_{\bar{\Omega}} \otimes I_{\Omega})] \quad (14)$$

being the post-measured state of the system, I_{Ω} is the identity operator in the Hilbert space of the qubits in Ω , and

$$p_k = \text{Tr}[(M_{\bar{\Omega}} \otimes I_{\Omega}) \rho (M_{\bar{\Omega}} \otimes I_{\Omega})] \quad (15)$$

is the probability of obtaining the measurement outcome k over the qubits in $\bar{\Omega}$. The definition of localizable entanglement depends on the existence of an entanglement measure E , referred to as the *seed measure* (cf. [46]), which can be computed for the post-measured state ρ_{Ω}^k over the subsystem Ω . Depending on the situation, E can either be a bipartite [36, 44, 45] or a multipartite entanglement measure [46, 49]. Unless otherwise stated, in this paper, we focus on computing the bipartite localizable entanglement over a subset Ω of qubits forming a non-trivial loop [7–9] of length $|\Omega|$, and we choose negativity [50, 51] as the seed measure.

It is generally difficult to compute localizable entanglement when the single-qubit measurements are to be performed over a large number $|\bar{\Omega}|$ of qubits, and analytical determination of the optimal measurement basis is possible only in few cases, eg. GHZ [46, 52] and W states [46, 53], Dicke states [46, 54], stabilizer states [36, 55], and a number of lattice spin models with certain symmetries [44, 45, 56]. In the cases of large quantum states ρ where the optimization of localizable entanglement can not be determined analytically, one can define a *restricted* localizable entanglement (RLE) [36, 47, 57], given by

$$E_{\Omega}^{RL} = \max_{\{M_{\bar{\Omega}}^{\sigma}\}} \sum_k p_k E(\rho_{\Omega}^k), \quad (16)$$

by confining the measurement basis for each qubit in $\bar{\Omega}$ to the eigenvectors of one of the three Pauli matrices σ^x , σ^y , and σ^z , where $\{M_{\bar{\Omega}}^{\sigma}\}$ is the complete set of all possible Pauli measurement configurations on all the qubits in $\bar{\Omega}$. The definitions of LE and RLE suggests that

$$E_{\Omega}^L \geq E_{\Omega}^{RL}, \quad (17)$$

where the same seed measure is chosen for computing both the LE and the RLE. While the equality in Eq. (17) occurs only in a few cases [36, 44–47, 57], there exists quantum states where the absolute deviation $\delta = |E_{\Omega}^L - E_{\Omega}^{RL}|$ from the actual value of the LE due to the restriction in the optimization is so small that the LE can be well-approximated using the RLE [47, 57], and analytical expressions for the RLE can also be determined.

Note that the optimization in RLE requires consideration of $3^{|\bar{\Omega}|}$ possible configurations of Pauli measurement setups, which can be difficult in situations where $|\bar{\Omega}|$ is a large number. However, one can choose a specific Pauli measurement setup from the complete set of $3^{|\bar{\Omega}|}$ configurations, where the choice depends on the structure of the quantum state (cf. [36, 55]), or the symmetry of the system (cf. [56]). While such a choice does not guarantee the optimized value of the

RLE for all possible values of the varying parameters in the system, a judicious choice would provide a lower bound, E'_{Ω} , of the RLE, such that the hierarchy in Eq. (17) becomes

$$E_{\Omega}^L \geq E_{\Omega}^{RL} \geq E'_{\Omega}, \quad (18)$$

where the bound

$$E'_{\Omega} = \sum_{k=0}^{2^{|\bar{\Omega}|-1}} p_k E(\rho_{\Omega}^k) \quad (19)$$

can be analytically computed in some cases (cf. [36]). Although the existence of a Pauli measurement setup over the qubits in $\bar{\Omega}$ corresponding to small values of the absolute deviations $\delta'_0 = |E_{\Omega}^L - E'_{\Omega}|$ and $\delta'_1 = |E_{\Omega}^{RL} - E'_{\Omega}|$ is not guaranteed, in the occasions where it exists, there are situations where the variations of E'_{Ω} as functions of the relevant parameters are qualitatively same as the variations of the LE and the RLE with the same parameters [36, 47, 57].

III. ON THE OPTIMAL BASIS FOR LOCALIZABLE ENTANGLEMENT

We now investigate the behaviour of localizable entanglement over a non-trivial loop in a topological quantum code when the strength of the parallel magnetic field is varied across a topological-to-non-topological quantum phase transition point.

Canonical measurement setup. Let us first consider the Kitaev model in a parallel field (Eq. (2)) on a square lattice with four plaquettes in 2×2 architecture, where the non-trivial loop in the $g \rightarrow 0$ limit of the Hamiltonian (2) is constituted of two qubits constructing the region Ω . The symmetry of the system implies identical value of LE computed over both horizontal and vertical non-trivial loops. We diagonalize H_K to obtain the ground state of the system, and numerically determine E_{Ω}^L and E_{Ω}^{RL} as functions of the magnetic field strength g . Our data suggests that for all values of g over a considerably wide range $[0, 2.0]$ across the quantum phase transition point, the optimization of the LE takes place in the Pauli basis, which is indicated by the vanishing δ (see Sec. II C) for all g . This is demonstrated by the coincidence of the graphs for E_{Ω}^L and E_{Ω}^{RL} in Fig. 2(a). At $g = 0$, a number of Pauli measurement setups can provide the optimized LE over the non-trivial loop [36]. One of the optimal Pauli measurement setups providing $E_{\Omega}^L = E_{\Omega}^{RL}$ at $g = 0$ has the following pattern (see Fig. 1(a)):

- (a) A qubit is measured in the σ^x basis if it is situated on a lattice edge that converges on the non-trivial loop, and
- (b) all other qubits are measured in the σ^z basis.

We refer to this as the *canonical measurement setup*. While the value of E'_{Ω} corresponding to this measurement setup coincides with E_{Ω}^L and E_{Ω}^{RL} at $g = 0$, with increasing g , its deviation δ'_0 from E_{Ω}^{RL} (see Sec. II C) increases at first, attains a maximum, and then decreases again, vanishing asymptotically at the limit $g \rightarrow \infty$ (see Fig. 2(c)). It is clear from

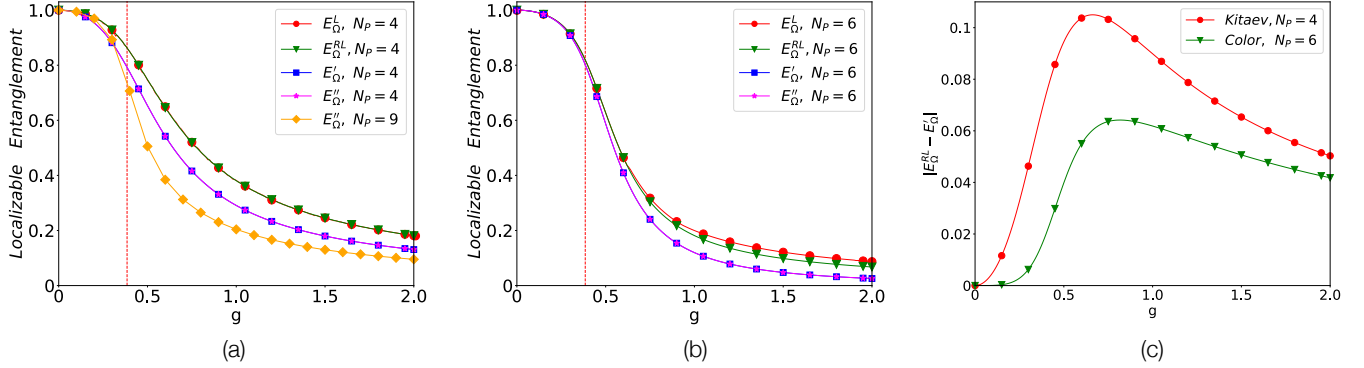


FIG. 2. (Color online) **Localizable entanglement vs. magnetic field strength.** Variations of localizable entanglement and its lower bounds in the noiseless scenario as functions of the parallel magnetic field strength g in the cases of (a) Kitaev code over a four- (2×2) and nine-plaquette (3×3) square lattice, and (b) color code over a six-plaquette (3×2) hexagonal lattice. The absolute error $|E_{\Omega}^{RL} - E'_{\Omega}|$ in the value of restricted localizable entanglement, when the measurements over $\bar{\Omega}$ are confined to the canonical measurement setup (see Sec. III) corresponding to the respective codes, are plotted as functions of g in (c). The dashed vertical line indicates the topological to non-topological quantum phase transition point g_c on the g axis, where $g_c = 0.328474(3)$ ($g_c = 0.385$) for Kitaev code (color code). In all graphs, localizable entanglement and its different lower bounds are computed over non-trivial loops. In the case of the Kitaev model, the vertical non-trivial loop of two qubits is chosen, while in the case of the color code, a horizontal non-trivial loop of four qubits form the subsystem Ω , where entanglement is computed over a $2 : 2$ bipartition.

Fig. 2(a) that the qualitative behaviour of E'_{Ω} as a function of g is the same as that of E_{Ω}^L and E_{Ω}^{RL} , and therefore E'_{Ω} reliably mimics the behaviour of the LE as a function of g across the quantum phase transition point g_c . Note that the measurement basis corresponding to canonical measurement setup on different qubits can be characterized by the relative positions of the qubits with respect to the non-trivial loop. In the subsequent sections, we will demonstrate the advantage of the canonical measurement setup in determining E'_{Ω} and a resource-optimized lower bound when the system size is large.

A resource-optimized lower bound for larger systems. Since the number of qubits in the system increases rapidly with increasing the lattice size, the number $2^{|\bar{\Omega}|}$ also grows very fast with the lattice, and the determination of E'_{Ω} becomes computationally demanding. In such situations, we define the following lower bound, which we refer to as the *resource-optimized localizable entanglement*, where only a *preferred set* \mathcal{K} of measurement outcomes occurring with a probability greater than a critical value p_c are considered:

$$E''_{\Omega} = \sum_{k \in \mathcal{K}} p_k E(\rho_{\Omega}^k) \quad \text{s.t. } p_k > p_c \quad \forall k \in \mathcal{K}. \quad (20)$$

Note that in the present problem, the nature of the ground state of H_K is qualitatively different in the cases of $g = 0$ (degenerate entangled ground state manifold of the topological code) and $g > 0$ (non-degenerate entangled ground state). Therefore, it is reasonable to expect that the preferred set \mathcal{K} corresponding to the set of probabilities $\{p_k\}$ such that $p_k > p_c \quad \forall k \in \mathcal{K}$ is different for $g = 0$ and $g > 0$. In order to take into account both situations, we consider the preferred set for the entire range of g to be $\mathcal{K} = \mathcal{K}_0 \cup \mathcal{K}_1 \cup \mathcal{K}_2 \cup \dots \cup \mathcal{K}_n$, where \mathcal{K}_0 (\mathcal{K}_i) is the preferred set of outcomes corresponding to $g = 0$ ($g = g_i > 0$, where we choose n non-zero positive values of

g). The number n and the value of p_c can be judiciously chosen depending on the situation, such that the error $|E'_{\Omega} - E''_{\Omega}|$ can be minimized depending on the available numerical resource. We test the performance of E''_{Ω} as a lower bound of LE in the case of the Kitaev model in a parallel magnetic field on a 2×2 square lattice, taking $n = 1$ with $g_1 = 2 \times 10^{-2}$, and setting $p_c = 10^{-10}$ for both \mathcal{K}_0 and \mathcal{K}_1 . We find that the absolute error $\epsilon = |E'_{\Omega} - E''_{\Omega}|$ is vanishing for all values of g in the range $[0, 2.0]$ (see Fig. 2(a)).

In order to estimate the performance of the resource-optimized lower bound (Eq. (20)), we compute the bound in the case of the Kitaev model in a parallel magnetic field on the square lattice of 9 plaquettes in a 3×3 architecture (see Fig. 1(a)) hosting a total of 18 qubits, where the non-trivial loop is constituted of 3 qubits, and one needs to consider 2^{15} measurement outcomes for computing E'_{Ω} . Considering the canonical measurement setup, we set $n = 1$, $g_1 = 2 \times 10^{-2}$ and $p_c = 10^{-10}$ for constructing both \mathcal{K}_0 and \mathcal{K}_1 , which leads to a set \mathcal{K} of 2944 measurement outcomes. We perform sparse matrix calculation where matrix elements having a magnitude less than 10^{-8} are considered to be zero. The variation of E''_{Ω} computed in this fashion as a function of g is shown in Fig. 2(a), where the localizable negativity is computed in a $1 : 2$ bipartition over the three-qubit region Ω , 1 and 2 being the sizes of the partitions. Note that the translation symmetry of the system ensures that the value of localizable entanglement is independent of which of the possible three $1 : 2$ partitions of the three-qubit region is chosen. It is clear from the figure that the qualitative behaviour of E''_{Ω} as the function of g remains the same as in the case of the four-plaquette system, and has a non-zero value over the considered range $g \in [0, 2.0]$ (see Fig. 2(a)), implying a non-zero LE over the said range.

We point out here that each measurement outcome in the

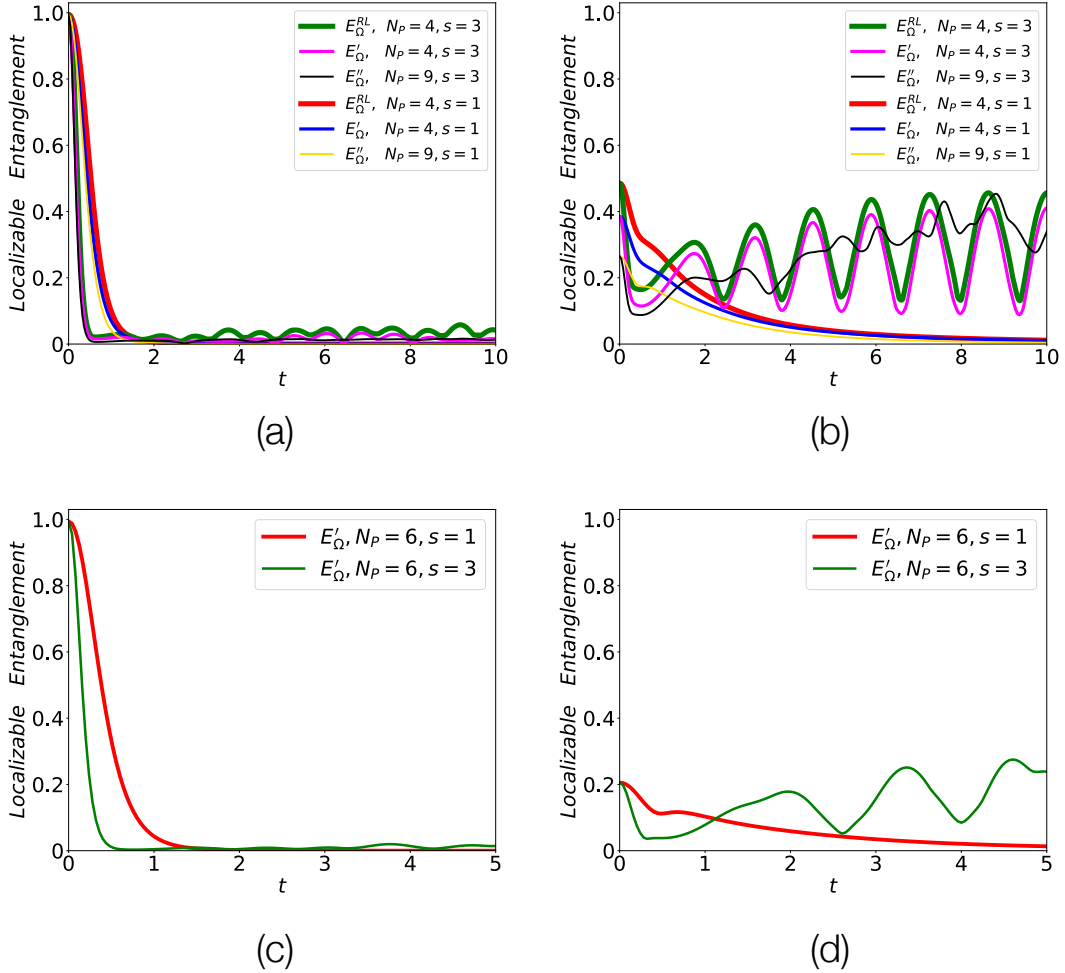


FIG. 3. (Color online) **Markovian and non-Markovian dynamics of localizable entanglement.** Variation of localizable entanglement and its lower bounds as functions of t in the case of Markovian ($s = 1$) and non-Markovian ($s = 3$) dephasing noise, when the initial states of the dynamics are taken from the topological ((a)-(c), $g = 10^{-1}$) and non-topological ((b)-(d), $g = 8 \times 10^{-1}$) phases of the Kitaev ((a)-(b)) and the color ((c)-(d)) code in the presence of parallel magnetic field. The Kitaev model is defined on a four-plaquette (2×2) and a nine-plaquette (3×3) square lattice, while the color code is defined on a six-plaquette (3×2) hexagonal lattice. The localizable entanglement and its lower bounds are computed over a non-trivial vertical loop constituted of two qubits in the case of the Kitaev code, and over a non-trivial horizontal loop of four qubits in the $2 : 2$ bipartition in the case of the color code.

expression (20) corresponds to a specific set of projection operations on all qubits in $\bar{\Omega}$. Assisted by the projection operation, a non-zero entanglement may exist only among all, or a subset of the qubits in Ω (cf. [58] where a cooling effect induced by the projection operators is used to compute bipartite entanglement in a frustrated system). We compute a bipartite entanglement measure E over the state ρ_{Ω}^k of the qubits in Ω , and find that for all measurement outcomes k such that $p_k > p_c$ and $E(\rho_{\Omega}^k) > 0$ at $g = 0$, $E(\rho_{\Omega}^k)$ behaves in a qualitatively similar way as in the case of E'_{Ω} and E''_{Ω} with increasing g . Therefore $E(\rho_{\Omega}^k)$ has the potential to mimic the behavior of LE with the increasing strength of the magnetic field, which can be easier to access experimentally when the system size is large.

We also test the resource-optimized lower bounds of LE for the color code in a parallel magnetic field (Eq. (7)) on a

hexagonal lattice. In this case, the canonical measurement setup is taken to be such that (see Fig. 1(b))

- (a) all qubits connected directly to the non-trivial loop with a lattice edge are measured in the σ^x basis, and
- (b) the rest of the qubits in $\bar{\Omega}$ are measured in the σ^z basis.

Fig. 2(b) depicts the variations of E_{Ω}^L , E_{Ω}^{RL} , and E'_{Ω} , as functions of g in the case of a 6 plaquette (3×2) hexagonal lattice, where entanglement is localized over the horizontal non-trivial loop formed by four qubits, and localizable negativity is computed over the $2 : 2$ bipartition, 2 being the sizes of each partition. Qualitatively similar results can also be obtained in the case of a $1 : 3$ bipartition of Ω . Note that in contrast to the Kitaev code, the value of RLE deviates from that of LE as g increases, although for $g \rightarrow \infty$ $E_{\Omega}^L = E_{\Omega}^{RL} = 0$. The

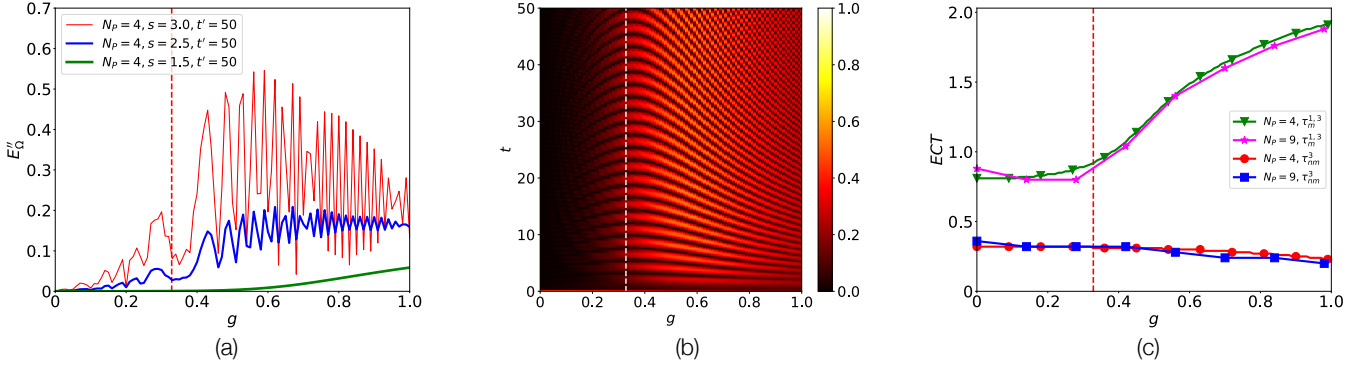


FIG. 4. (Color online) **Distinguishing topological phase from the non-topological phase.** (a) Variation of E''_{Ω} as a function of g at $t' = 50$ across the topological to non-topological quantum phase transition point. (b) E''_{Ω} as a function of g and t . (c) The variations of ECTs, τ_{NM}^3 and $\tau_M^{1,3}$, as functions of g across the quantum phase transition point. Figures (a) and (b) are for the Kitaev model in a parallel magnetic field on a 2×2 square lattice, while figure (c) contains data for the same model on a 2×2 and a 3×3 square lattice. In all the figures, the quantum phase transition point is marked by the dashed vertical line. The value of E_C^3 for computing the ECTs for the Markovian and the non-Markovian dephasing noise is $E_C^3 = 0.14$ for the 2×2 square lattice, and $E_C^3 = 0.11$ for the 3×3 square lattice.

variation of $\epsilon |E_{\Omega}^{RL} - E'_{\Omega}|$ as a function of g , on the other hand, remains qualitatively similar to that of the Kitaev model in a parallel field (see Fig. 2(c)). For computing E''_{Ω} , we set values of n , g_i , and p_c similar to the case of the Kitaev model, and find that these choices lead to the cardinality of the set \mathcal{K} to be $2^{|\bar{\Omega}|}$, where $|\bar{\Omega}| = 8$ in the present case, yielding the same value for both E'_{Ω} and E''_{Ω} throughout the range $g \in [0, 2.0]$ (see Fig. 2(b)).

IV. LOCALIZABLE ENTANGLEMENT UNDER DEPHASING NOISE

In this section, we discuss the effect of single qubit dephasing noise on the bipartite localizable entanglement over a non-trivial loop of the topological code in the presence of parallel magnetic field. We also demonstrate how the dynamics of localizable entanglement can be used to differentiate between the topological and non-topological phases of the models. We determine the time-dependent state ρ of the system by numerically solving the quantum master equation (Eq. (11)) using the Runge-Kutta 4th order method with the ground state of the system as the initial state ($t = 0$) ρ_0 , and then compute the localizable entanglement and its lower bounds as a function of t on a set Ω of qubits forming a non-trivial loop. In the case of large systems, we use sparse matrix calculations to determine ρ as a function of t . More specifically, in the case of the 9-plaquette Kitaev code, we set density matrix elements to be zero if its magnitude is $< 10^{-8}$.

Dynamics of localizable entanglement and collapse time. To demonstrate the results, we use the Kitaev model in a parallel magnetic field on a four plaquette square lattice in the 2×2 architecture. In Fig. 3(a)-(b), we depict the variations of E_{Ω}^{RL} and E'_{Ω} as functions of t in the case of the Markovian ($s < 2$) and non-Markovian ($s > 2$) dephasing noise, where we choose the initial state ρ_0 to be the ground state of the system in the topological phase ($g < g_c$) (Fig. 3(a)) and the non-

topological phase ($g > g_c$) (Fig. 3(b)). We further compute E'_{Ω} for all values of t by using the canonical measurement setup on the qubits in $\bar{\Omega}$. We also compute E''_{Ω} by setting the values of n , g_1 , and p_c to be the same as described in Sec. III in the noiseless case of the Kitaev code under parallel magnetic field. We find that

$$E_{\Omega}^L = E_{\Omega}^{RL} \geq E'_{\Omega} = E''_{\Omega} \quad (21)$$

for the full range of t considered in the paper, in the case of both Markovian and non-Markovian dephasing noise, and for initial states from both the topological and the non-topological phase.

We also compute E''_{Ω} as a function of t in the case of a 9-plaquettes Kitaev code in parallel magnetic field to find that the dynamical behaviour of E''_{Ω} remains qualitatively same as in the four-plaquettes case (see Fig. 3(a)-(b)), where we have kept the values of n , g_1 , and p_c the same as in the noiseless scenario (see Sec. III). In all our calculations, for the purpose of demonstration, we fix $s = 1$ for Markovian and $s = 3$ for non-Markovian dephasing noise. However, the results for the Markovian (non-Markovian) noise remain qualitatively unchanged for all values of s in the appropriate range $0 < s < 2$ ($2 < s \leq 3$) (cf. [41, 42]), only the amplitude of oscillations of the LE and its lower bounds increasing with an increase in s for $s > 2$.

Our numerical results indicate that in the case of the non-Markovian noise ($s > 2$), the LE and its lower bounds decreases monotonically to a non-zero value E_C^s at first, and then starts oscillating (see Fig. 3(a)-(b)), the amplitude of oscillation being considerably larger when the initial state of the dynamics is chosen from the non-topological phase. The superscript in E_C^s indicates the value of the Ohmicity parameter. The *entanglement collapse time* (ECT), for a fixed value of $s > 2$, is defined as the time $t = \tau_{NM}^s$ at which the value of, for example, RLE, collapses to its respective E_C^s value for the first time, such that the landscape of RLE has its first *trough* at $t = \tau_{NM}^s$. For a fixed value of s , the value of τ_{NM}^s can be

obtained as the solution of

$$E_{\Omega}^{RL}(t) = E_C^s, \quad (22)$$

where we have used E_{Ω}^{RL} for demonstration, and similar equations can be written for the LE and all of its lower bounds. In situations where the value of the RLE (or any other lower bound) remains at E_C^s for a finite interval of time, τ_{NM}^s is defined as the first time instant when $E_{\Omega}^{RL}(t) = E_C^s$. In contrast, in the case of the Markovian noise, magnitude of LE and its lower bounds decrease monotonically with time, and eventually vanishes. In order to compare the collapse of LE and its lower bounds with the case of non-Markovian noise denoted by a fixed value of $s > 2$, in the case of Markovian noise denoted by an Ohmicity $s' < 2$, we determine the ECT, $\tau_M^{s',s}$ as the time at which the value of LE or one of its lower bound, for the first time, collapses to its respective E_C^s value corresponding to the non-Markovian noise. For instance, in the case of the RLE, the value of $\tau_M^{s',s}$ can be obtained as the solution of $E_{\Omega}^{RL}(t) = E_C^s$, where $E_{\Omega}^{RL}(t)$ corresponds to the case of the Markovian noise with Ohmicity s' . Once again, we have used RLE for demonstration, while the definition of $\tau_M^{s',s}$ is similar for LE and all of its lower bounds under Markovian noise. We comment on the behaviour of τ_{NM}^s and $\tau_M^{s',s}$ as functions of g in the subsequent discussions.

Distinguishing phases from the dynamics

It is clear from Figs. 3(a)-(b) that in the case of the non-Markovian dephasing noise, the magnitudes of oscillations and the value of E_C^s corresponding to the LE and its lower bounds are considerably higher when the initial state of the dynamics is chosen from the non-topological phase, compared to the same when the initial state of the system is taken from the topological phase. It implies that the dynamics of LE and its lower bounds under Markovian and non-Markovian dephasing noise can be categorized by the initial state ($t = 0$) of the dynamics, which is characteristic to the phases of the system. This feature can be used to distinguish between the phases of topological codes in the presence of parallel magnetic field in situations where single-qubit dephasing noise is present in the system, and one is forced to investigate the phases after a long time has elapsed. The dynamical behaviours of LE and its lower bounds imply that in the case of single-qubit non-Markovian dephasing noise in large Kitaev codes under parallel magnetic field, it is sufficient to investigate E_{Ω}'' in order to distinguish between the topological and the non-topological phases. The important points of the phase discrimination in this method are as follows.

- (a) Let us choose a large time $t = t'$, at which $E_{\Omega}''(t')$ is computed. The crossover from the topological to the non-topological phase of the system at $g = g_c$ is distinguished by the onset of large temporal oscillations of E_{Ω}'' , as depicted in Fig. 4(a) in the case of a four-plaquette system. As the value of the Ohmicity increases, the amplitude of oscillations become larger.

- (b) The large time t' can be chosen according to the situation in hand. In Fig. 4(a), we have demonstrated $E_{\Omega}''(t')$ vs. g variations for $t' = 50$, such that in the non-topological phase, $t' \gg \tau_{NM}^s$. Our numerical analysis suggests that the oscillations are larger for moderately low values of g in the non-topological phase of the system, while the oscillation gradually dies out as the initial state approaches towards a product state by increasing the value of g .
- (c) Fig. 4(b) depicts the variation of E_{Ω}'' as a function of g and t , where the repetitive revivals and collapses of E_{Ω}'' with g at large times are clearly seen in the non-topological phase of the Kitaev code in a parallel magnetic field on a 4-plaquette square lattice. Our numerical analysis of the 9-plaquette system indicates that the qualitative trend of E_{Ω}'' vs. g and t remains the same as one goes higher in the system size.
- (d) It is important to understand how the characteristic ECTs $\tau_M^{s',s}$ and τ_{NM}^s corresponding to the Markovian and non-Markovian dynamics of LE and its lower bounds vary with g . In Fig. 4(c), we plot $\tau_M^{1,3}$ and τ_{NM}^3 as functions of g , for the four plaquette lattice. The ECT $\tau_M^{1,3}$ for the non-Markovian noise remains effectively constant in the topological phase, then starts increasing across the quantum phase transition point into the topological phase as g increases, thereby distinguishing the two phases. In contrast, τ_{NM}^3 remains almost constant across the quantum phase transition, and then decreases slowly with increasing g . These trends also remain the same as one increases the system size, as is demonstrated in Fig. 4(c).

Distinguishing Markovianity from non-Markovianity. We point out here that knowledge about the phases of the Kitaev model in a parallel magnetic field can also be used to distinguish between the Markovian and non-Markovian type of the dephasing noise using the dynamics of the proposed lower bound (Eq. (20)). Starting from a ground state of the model in the non-topological phase as the initial state, at $t = t'$, if a highly oscillating behavior with high amplitude (mildly oscillating behaviour with low amplitude) of E_{Ω}'' is found, then the noise is non-Markovian (Markovian). Such a distinction can be useful in situations where the single qubit noise is known to be dephasing, but the Markovianity of the noise is not decided.

In order to examine whether the features reported above are model-specific, we also test these findings in the case of the color code in a parallel magnetic field on a hexagonal lattice under periodic boundary condition. We demonstrate the dynamics of E_{Ω}' in Figs. 3(c)-(d) under the Markovian ($s = 1$) and non-Markovian ($s = 3$) dephasing noise when the initial state is chosen from the topological (Fig. 3(c)) and the non-topological (Fig. 3(d)) phases of the model. We find that $E_{\Omega}' = E_{\Omega}''$ for the entire range of time considered, where we have computer E_{Ω}' using the canonical measurement setup for the color code (see Sec. III), setting the values of n , g_1 , and p_c similar to that reported in Sec. III. The qualitative behaviours

of E'_Ω vs. t remains the same as the Kitaev model under parallel magnetic field, as is evident from Figs. 3(c)-(d). We also investigate whether the topological and the non-topological phases in the color code under parallel field can be distinguished using the dynamics of E''_Ω , and find that all the phase-discriminating features including (a) the large amplitude oscillations of E''_Ω as a function of g in the non-topological phase at a long time $t' \gg \tau_{NM}^s$, and (b) the increase of $\tau_M^{s',s}$ as a function of g across the topological to non-topological quantum phase transition point are present also in the case of the color code under parallel magnetic field. This highlights the importance of these findings in distinguishing topological phase from the non-topological phase in the case of topological quantum codes under parallel magnetic field.

V. CONCLUSIONS

Topological quantum codes such as the Kitaev code and the color code have attracted a lot of attentions due to their immense potential in performing quantum computation tasks. In the presence of external perturbations like local magnetic field, these models exhibit topological order at the zero field limit, which is robust against small perturbations. However, with the increase of the perturbation strength, the model undergoes a topological to non-topological quantum phase transition, and the ground state becomes fully polarized when the field strength is infinite. The topological phase and the corresponding quantum phase transition can not be characterized by local order parameters and spontaneous symmetry breaking. In this paper, we investigate the topological to non-topological quantum phase transition occurring in a topological quantum code in the presence of a parallel magnetic field in terms of the entanglement localized over a non-trivial loop

via local projection measurements on spins outside the loop, and its dynamics due to single-qubit dephasing noise present in the system. In the noiseless scenario, we identify a canonical Pauli measurement setup that can optimize a lower bound of localizable entanglement restricted by confining the local measurement basis to Pauli basis only. Using the canonical basis, we define a resource-optimized lower bound of localizable entanglement which can be computed for larger topological codes according to the available numerical resource. We demonstrate that in the case of the non-Markovian noise, starting with an initial state of the system from the non-topological phase, the resource optimized lower bound exhibits oscillations with high amplitude at large time, while the oscillation is suppressed if the initial state is chosen from the topological phase. Our numerical investigation of this phenomena for the Kitaev code and the color code of different sizes shows that this dynamical feature of the lower bound of localizable entanglement can be used to distinguish between the topological and the non-topological phases of the topological quantum codes under parallel magnetic field. These findings are expected to be useful in investigating phases of topological systems during the evolution of the system due to the presence of local noise.

ACKNOWLEDGMENTS

We acknowledge the support from the Science and Engineering Research Board (SERB), India through the Start-Up Research Grant (SRG) (File No. - SRG/2020/000468 Date: 11 November 2020), and the use of **QIClib** – a modern C++ library for general purpose quantum information processing and quantum computing. AKP acknowledges IIT Palakkad for the Seed Grant, and thanks Aditi Sen(De) for useful discussions.

-
- [1] J. Preskill, [arXiv:1203.5813](https://arxiv.org/abs/1203.5813) (2012).
- [2] A. W. Harrow and A. Montanaro, *Nature* **549**, 203 (2017).
- [3] F. Arute, K. Arya, R. Babbush, D. Bacon, J. C. Bardin, R. Barends, R. Biswas, S. Boixo, F. G. S. L. Brandao, D. A. Buell, B. Burkett, Y. Chen, Z. Chen, B. Chiaro, R. Collins, W. Courtney, A. Dunsworth, E. Farhi, B. Foxen, A. Fowler, C. Gidney, M. Giustina, R. Graff, K. Guerin, S. Habegger, M. P. Harrigan, M. J. Hartmann, A. Ho, M. Hoffmann, T. Huang, T. S. Humble, S. V. Isakov, E. Jeffrey, Z. Jiang, D. Kafri, K. Kechedzhi, J. Kelly, P. V. Klimov, S. Knysh, A. Korotkov, F. Kostritsa, D. Landhuis, M. Lindmark, E. Lucero, D. Lyakh, S. Mandrà, J. R. McClean, M. McEwen, A. Megrant, X. Mi, K. Michielsen, M. Mohseni, J. Mutus, O. Naaman, M. Neeley, C. Neill, M. Y. Niu, E. Ostby, A. Petukhov, J. C. Platt, C. Quintana, E. G. Rieffel, P. Roushan, N. C. Rubin, D. Sank, K. J. Satzinger, V. Smelyanskiy, K. J. Sung, M. D. Trevithick, A. Vainsencher, B. Villalonga, T. White, Z. J. Yao, P. Yeh, A. Zalcman, H. Neven, and J. M. Martinis, *Nature* **574**, 505 (2019).
- [4] D. P. DiVincenzo, *Fortschr. Phys.* **48**, 771 (2000); D. Gottesman, in *Quantum information science and its contributions to mathematics, Proceedings of Symposia in Applied Mathematics*, Vol. 68 (2010) pp. 13–58.
- [5] K. Fujii, [arXiv:1504.01444](https://arxiv.org/abs/1504.01444) (2015).
- [6] C. Nayak, S. H. Simon, A. Stern, M. Freedman, and S. Das Sarma, *Rev. Mod. Phys.* **80**, 1083 (2008); J. K. Pachos and S. H. Simon, *New J. Phys.* **16**, 065003 (2014); V. Lahtinen and J. K. Pachos, *SciPost Phys.* **3**, 021 (2017).
- [7] E. Dennis, A. Kitaev, A. Landahl, and J. Preskill, *J. Math. Phys.* **43**, 4452 (2002).
- [8] A. Kitaev, *Ann. Phys.* **303**, 2 (2003); *Ann. Phys.* **321**, 2 (2006).
- [9] H. Bombin and M. A. Martin-Delgado, *Phys. Rev. Lett.* **97**, 180501 (2006); *Phys. Rev. Lett.* **98**, 160502 (2007).
- [10] T. M. Stace, S. D. Barrett, and A. C. Doherty, *Phys. Rev. Lett.* **102**, 200501 (2009); T. M. Stace and S. D. Barrett, *Phys. Rev. A* **81**, 022317 (2010); D. Vodola, D. Amaro, M. A. Martin-Delgado, and M. Müller, *Phys. Rev. Lett.* **121**, 060501 (2018); R. Stricker, D. Vodola, A. Erhard, L. Postler, M. Meth, M. Ringbauer, P. Schindler, T. Monz, M. Müller, and R. Blatt, *Nature* **585**, 207 (2020).
- [11] J. R. Wootton and J. K. Pachos, *Phys. Rev. Lett.* **107**, 030503 (2011).
- [12] H. G. Katzgraber, H. Bombin, and M. A. Martin-Delgado, *Phys. Rev. Lett.* **103**, 090501 (2009).

- [13] D. Nigg, M. Müller, E. A. Martinez, P. Schindler, M. Hennrich, T. Monz, M. A. Martin-Delgado, and R. Blatt, *Science* **345**, 302 (2014).
- [14] N. M. Linke, M. Gutierrez, K. A. Landsman, C. Figgatt, S. Debnath, K. R. Brown, and C. Monroe, *Sci. Adv.* **3**, 10 (2017); K. Wright, K. M. Beck, S. Debnath, J. M. Amini, Y. Nam, N. Grzesiak, J.-S. Chen, N. C. Pisenti, M. Chmielewski, C. Collins, K. M. Hudek, J. Mizrahi, J. D. Wong-Campos, S. Allen, J. Apisdorf, P. Solomon, M. Williams, A. M. Ducore, A. Blinov, S. M. Kreikemeier, V. Chaplin, M. Keesan, C. Monroe, and J. Kim, [arXiv:1903.08181](https://arxiv.org/abs/1903.08181) (2019).
- [15] J. Kelly, R. Barends, A. G. Fowler, A. Megrant, E. Jeffrey, T. C. White, D. Sank, J. Y. Mutus, B. Campbell, Y. Chen, Z. Chen, B. Chiaro, A. Dunsworth, I.-C. Hoi, C. Neill, P. J. J. O'Malley, C. Quintana, P. Roushan, A. Vainsencher, J. Wenner, A. N. Cleland, and J. M. Martinis, *Nature* **519**, 66 (2015); J. M. Gambetta, J. M. Chow, and M. Steffen, *Nature Phys. J. Quant. Inf.* **3**, 2 (2017).
- [16] J. Preskill, *Quantum* **2**, 79 (2018); A. Paler, A. Zulehner, and R. Wille, [arXiv:1806.07241](https://arxiv.org/abs/1806.07241) (2018); B. Nash, V. Gheorghiu, and M. Mosca, [arXiv:1904.01972](https://arxiv.org/abs/1904.01972) (2019).
- [17] S. Trebst, P. Werner, M. Troyer, K. Shtengel, and C. Nayak, *Phys. Rev. Lett.* **98**, 070602 (2007); F. Wu, Y. Deng, and N. Prokof'ev, *Phys. Rev. B* **85**, 195104 (2012).
- [18] S. Dusuel, M. Kamfor, R. Orús, K. P. Schmidt, and J. Vidal, *Phys. Rev. Lett.* **106**, 107203 (2011); M. H. Zarei, *Phys. Rev. B* **100**, 125159 (2019); D. I. Tsomokos, T. J. Osborne, and C. Castelnovo, *Phys. Rev. B* **83**, 075124 (2011).
- [19] R. Wiedmann, L. Lenke, M. R. Walther, M. Mühlhauser, and K. P. Schmidt, *Phys. Rev. B* **102**, 214422 (2020); V. Karimipour, L. Memarzadeh, and P. Zarkeshian, *Phys. Rev. A* **87**, 032322 (2013).
- [20] A. Jamadagni, H. Weimer, and A. Bhattacharyya, *Phys. Rev. B* **98**, 235147 (2018).
- [21] M. H. Zarei, *Phys. Rev. A* **91**, 022319 (2015); S. S. Jahromi, M. Kargarian, S. F. Masoudi, and K. P. Schmidt, *Phys. Rev. B* **87**, 094413 (2013).
- [22] R. B. Laughlin, *Phys. Rev. Lett.* **50**, 1395 (1983).
- [23] X. G. Wen and Q. Niu, *Phys. Rev. B* **41**, 9377 (1990); X.-G. Wen, *Advances in Physics* **44**, 405 (1995), <https://doi.org/10.1080/00018739500101566>.
- [24] L. D. Landau, *Phys. Z. Sowjetunion* **11**, 26 (1937); N. Goldenfeld, *Lectures on Phase Transitions and Critical Phenomena* (Perseus Books, Boston, 1992).
- [25] R. Horodecki, P. Horodecki, M. Horodecki, and K. Horodecki, *Rev. Mod. Phys.* **81**, 865 (2009).
- [26] K. Modi, A. Brodutch, H. Cable, T. Paterek, and V. Vedral, *Rev. Mod. Phys.* **84**, 1655 (2012); A. Bera, T. Das, D. Sadhukhan, S. S. Roy, A. Sen(De), and U. Sen, *Reports on Progress in Physics* **81**, 024001 (2017).
- [27] C. H. Bennett, G. Brassard, C. Crépeau, R. Jozsa, A. Peres, and W. K. Wootters, *Phys. Rev. Lett.* **70**, 1895 (1993); D. Bouwmeester, J.-W. Pan, K. Mattle, M. Eibl, H. Weinfurter, and A. Zeilinger, *Nature* **390**, 575 (1997).
- [28] C. H. Bennett and S. J. Wiesner, *Phys. Rev. Lett.* **69**, 2881 (1992); K. Mattle, H. Weinfurter, P. G. Kwiat, and A. Zeilinger, *Phys. Rev. Lett.* **76**, 4656 (1996); A. Sen(De) and U. Sen, *Phys. News* **40**, 17 (2011), [arXiv:1105.2412](https://arxiv.org/abs/1105.2412).
- [29] A. K. Ekert, *Phys. Rev. Lett.* **67**, 661 (1991); T. Jennewein, C. Simon, G. Weihs, H. Weinfurter, and A. Zeilinger, *Phys. Rev. Lett.* **84**, 4729 (2000); R. Raussendorf and H. J. Briegel, *Phys. Rev. Lett.* **86**, 5188 (2001); R. Raussendorf, D. E. Browne, and H. J. Briegel, *Phys. Rev. A* **68**, 022312 (2003); H. J. Briegel, D. E. Browne, W. Dür, R. Raussendorf, and M. Van den Nest, *Nat. Phys.* **5**, 19 (2009).
- [30] L. Amico, R. Fazio, A. Osterloh, and V. Vedral, *Rev. Mod. Phys.* **80**, 517 (2008); G. D. Chiara and A. Sanpera, *Reports on Progress in Physics* **81**, 074002 (2018).
- [31] S. O. Skovsveth and S. D. Bartlett, *Phys. Rev. A* **80**, 022316 (2009); P. Smacchia, L. Amico, P. Facchi, R. Fazio, G. Florio, S. Pascazio, and V. Vedral, *Phys. Rev. A* **84**, 022304 (2011).
- [32] S. Montes and A. Hamma, *Phys. Rev. E* **86**, 021101 (2012).
- [33] M. Kargarian, *Phys. Rev. A* **78**, 062312 (2008).
- [34] D. Leibfried, R. Blatt, C. Monroe, and D. Wineland, *Rev. Mod. Phys.* **75**, 281 (2003); D. Leibfried, E. Knill, S. Seidelin, J. Britton, R. B. Blakestad, J. Chiaverini, D. B. Hume, W. M. Itano, J. D. Jost, C. Langer, R. Ozeri, R. Reichle, and D. J. Wineland, *Nature* **438**, 639 (2005); K. R. Brown, J. Kim, and C. Monroe, *Nature Phys. J. Quant. Inf.* **2**, 16034 EP (2016).
- [35] J. Clarke and F. K. Wilhelm, *Nature* **453**, 1031 (2008); A. J. Berkley, H. Xu, R. C. Ramos, M. A. Gubrud, F. W. Strauch, P. R. Johnson, J. R. Anderson, A. J. Dragt, C. J. Lobb, and F. C. Wellstood, *Science* **300**, 1548 (2003).
- [36] D. Amaro, M. Müller, and A. K. Pal, *New J. Phys.* **20**, 063017 (2018); *New Journal of Physics* **22**, 053038 (2020).
- [37] H.-P. Breuer and F. Petruccione, *The Theory of Open Quantum Systems* (Oxford University Press, Oxford, 2002); A. Rivas and S. F. Huelga, *Open Quantum Systems: An Introduction* (Springer Briefs in Physics, Springer, Berlin, 2012); Á. Rivas, S. F. Huelga, and M. B. Plenio, *Reports on Progress in Physics* **77**, 094001 (2014).
- [38] K. Życzkowski, P. Horodecki, M. Horodecki, and R. Horodecki, *Phys. Rev. A* **65**, 012101 (2001); L. Diósi, "Progressive decoherence and total environmental disentanglement," in *Irreversible Quantum Dynamics*, edited by F. Benatti and R. Floreanini (Springer Berlin Heidelberg, Berlin, Heidelberg, 2003) pp. 157–163; P. J. Dodd and J. J. Halliwell, *Phys. Rev. A* **69**, 052105 (2004); M. P. Almeida, F. de Melo, M. Hor-Meyll, A. Salles, S. P. Walborn, P. H. S. Ribeiro, and L. Davidovich, *Science* **316**, 579 (2007), <https://science.sciencemag.org/content/316/5824/579.full.pdf>; A. Salles, F. de Melo, M. P. Almeida, M. Hor-Meyll, S. P. Walborn, P. H. Souto Ribeiro, and L. Davidovich, *Phys. Rev. A* **78**, 022322 (2008); T. Yu and J. H. Eberly, *Science* **323**, 598 (2009), <https://science.sciencemag.org/content/323/5914/598.full.pdf>.
- [39] C. Castelnovo and C. Chamon, *Phys. Rev. B* **76**, 184442 (2007); *Phys. Rev. B* **78**, 155120 (2008); A. T. Schmitz, S.-J. Huang, and A. Prem, *Phys. Rev. B* **99**, 205109 (2019).
- [40] J. Łuczka, *Physica A: Statistical Mechanics and its Applications* **167**, 919 (1990); G. M. Palma, K.-a. Suominen, and A. Ekert, *Proceedings of the Royal Society of London. Series A: Mathematical, Physical and Engineering Sciences* **452**, 567 (1996); J. H. Reina, L. Quiroga, and N. F. Johnson, *Phys. Rev. A* **65**, 032326 (2002).
- [41] P. Haikka, S. McEndoo, G. De Chiara, G. M. Palma, and S. Maniscalco, *Phys. Rev. A* **84**, 031602 (2011).
- [42] P. Haikka, T. H. Johnson, and S. Maniscalco, *Phys. Rev. A* **87**, 010103 (2013).
- [43] D. P. DiVincenzo, C. A. Fuchs, H. Mabuchi, J. A. Smolin, A. Thapliyal, and A. Uhlmann, [arXiv:quant-ph/9803033](https://arxiv.org/abs/quant-ph/9803033) (1998).
- [44] F. Verstraete, M. Popp, and J. I. Cirac, *Phys. Rev. Lett.* **92**, 027901 (2004); M. Popp, F. Verstraete, M. A. Martín-Delgado, and J. I. Cirac, *Phys. Rev. A* **71**, 042306 (2005).
- [45] F. Verstraete, M. A. Martín-Delgado, and J. I. Cirac, *Phys. Rev. Lett.* **92**, 087201 (2004); B.-Q. Jin and V. E. Korepin, *Phys. Rev. A* **69**, 062314 (2004).

- [46] D. Sadhukhan, S. S. Roy, A. K. Pal, D. Rakshit, A. Sen(De), and U. Sen, *Phys. Rev. A* **95**, 022301 (2017).
- [47] R. Banerjee, A. K. Pal, and A. Sen(De), *Phys. Rev. A* **101**, 042339 (2020).
- [48] A. Acín, J. I. Cirac, and M. Lewenstein, *Nat. Phys.* **3**, 256 (2007).
- [49] A. Streltsov, S. Lee, and G. Adesso, *Phys. Rev. Lett.* **115**, 030505 (2015).
- [50] **Negativity.** Normalized negativity for a bipartite quantum state ρ_{AB} is defined as $\mathcal{N}(\rho_{AB}) = (||\rho_{AB}^{T_A}|| - 1)/(d - 1)$, where $d = \min\{d_A, d_B\}$, d_A (d_B) being the dimension of the Hilbert space associated to the partition A (B), $||\varrho|| = \text{Tr}\sqrt{\varrho^\dagger\varrho}$ is the trace norm of the density operator ϱ , and $\rho_{AB}^{T_A}$ is obtained by performing partial transposition of ρ_{AB} w.r.t. the party A [51].
- [51] A. Peres, *Phys. Rev. Lett.* **77**, 1413 (1996); M. Horodecki, P. Horodecki, and R. Horodecki, *Phys. Lett. A* **223**, 1 (1996); G. Vidal and R. F. Werner, *Phys. Rev. A* **65**, 032314 (2002); B. Leggio, A. Napoli, H. Nakazato, and A. Messina, *Entropy* **22** (2020), 10.3390/e22010062.
- [52] D. M. Greenberger, M. A. Horne, and A. Zeilinger, *Bell's theorem, quantum theory and conceptions of the universe* (Kluwer, Netherlands, 1989).
- [53] A. Zeilinger, M. A. Horne, and D. M. Greenberger, in *Proceedings of Squeezed States and Quantum Uncertainty*, Vol. 73 (NASA Conf. Publ, 1992) p. 3135; W. Dür, G. Vidal, and J. I. Cirac, *Phys. Rev. A* **62**, 062314 (2000).
- [54] R. H. Dicke, *Phys. Rev.* **93**, 99 (1954); A. Kumar, H. S. Dhar, R. Prabhu, A. Sen(De), and U. Sen, *Physics Letters A* **381**, 1701 (2017).
- [55] M. Hein, J. Eisert, and H. J. Briegel, *Phys. Rev. A* **69**, 062311 (2004); M. Hein, W. Dür, J. Eisert, R. Raussendorf, M. Van den Nest, and H. J. Briegel, [arXiv:quant-ph/0602096](https://arxiv.org/abs/quant-ph/0602096) (2006).
- [56] L. C. Venuti and M. Roncaglia, *Phys. Rev. Lett.* **94**, 207207 (2005).
- [57] R. Banerjee, A. K. Pal, and A. Sen(De), [arXiv:2003.02175](https://arxiv.org/abs/2003.02175) (2020).
- [58] A. Sen(De), U. Sen, J. Dziarmaga, A. Sanpera, and M. Lewenstein, *Phys. Rev. Lett.* **101**, 187202 (2008).